Equilibration and filtering of quantum Hall edge states in few-layer black phosphorus

Jiawei Yang,[1] Kangyu Wang,[1] Shi Che,[1] Zachary J. Tuchfeld,[1] Kenji Watanabe,[2] Takashi Taniguchi,[3] Dmitry Shcherbakov,[1] Seongphil Moon,[4] Dmitry Smirnov,[4] Ruoyu Chen,[1] Marc Bockrath,[1] and Chun Ning Lau[1,*]

[1]*Department of Physics, Ohio State University, Columbus, Ohio 43220, USA*

[2]*Research Center for Functional Materials, National Institute for Materials Science, 1-1 Namiki, Tsukuba 305-0044, Japan*

[3]*International Center for Materials Nanoarchitectonics, National Institute for Materials Science, 1-1 Namiki, Tsukuba 305-0044, Japan*

[4]*National High Magnetic Field Laboratory, Tallahassee, Florida 32310, USA*

(Received 17 August 2020; revised 18 October 2020; accepted 29 October 2020; published 24 November 2020; corrected 15 January 2021)

This paper is a contribution to the joint Physical Review Applied *and* Physical Review Materials *collection titled Two-Dimensional Materials and Devices.*

We realize p-p'-p junctions in few-layer black phosphorus devices, and use magnetotransport measurements to study the equilibration and transmission of edge states at the interfaces of regions with different charge densities. We observe both full equilibration, where all edge channels equilibrate and are equally partitioned at the interfaces, and partial equilibration, where equilibration only takes place among modes of the same spin polarization. Furthermore, the inner p' region with low-doping level in the junction can function as a filter for highly doped p regions which demonstrates gate-tunable transmission of edge channels.

DOI: 10.1103/PhysRevMaterials.4.114008

In a magnetic field, electron orbits in a two-dimensional electron system coalesce into Landau levels, giving rise to chiral quantum Hall edge (QH) states that propagate without dissipation. These edge states provide an attractive platform for exploring strong electron interactions, one-dimensional transport, interferometry, and resistance standard [1–4]. More recently, manipulation of these edge states has been proposed as a route for topological quantum computation [5–7].

In the past decade, atomically thin two-dimensional (2D) semiconductors have provided alluring platforms for control and manipulation of QH edge states, with advantages such as tunability of band gap, effective mass, and charge density [8–12]. In particular, atomically thin black phosphorus (BP) has been intensively studied due to its high electron mobility and a direct band gap that is tunable by electric field, layer, and strain, with a wide range of potential electronic, optoelectronic, and thermoelectric applications [13–24]. With recent improvement in materials and device preparation, we have recently achieved field effect mobility of up to 50 000 $\mathrm{cm}^2/\mathrm{V\,s}$ and 4000 $\mathrm{cm}^2/\mathrm{V\,s}$ in BP field effect transistor devices at low temperature and room temperature, respectively, and observed integer and fractional QH states under high magnetic field [13]. Yet, the interaction and equilibration of QH edge states in few-layer BP devices has not been studied.

Here we report magnetotransport measurements of few-layer black phosphorus devices with local gates, thus realizing p-p'-p junctions with tunable densities in different regions. In the QH regime, the equilibration of edge states at the interface of regions with different doping levels gives rise to integer and fractional plateaus in two-terminal conductance and four-terminal longitudinal resistance values. In devices with moderate mobility, the plateau values are well accounted for by a model that assumes full equilibration among all edge states. Surprisingly, in a device with higher mobility, the plateaus' values suggest separate, selective equilibration among channels with different spin polarization. When the outer p regions are highly doped, the junction can also serve as a gate-tunable quantum filter that can shut off the transmission channels one by one. The observation of partial equilibration and selective transmission of edge states in a 2D semiconductor underscores the potential afforded by 2D materials for exploring and harnessing different phenomena and applications.

We construct the black phosphorus devices by using polypropylene carbon (PPC) films to sequentially pick up hexagonal boron nitride (hBN), BP, and hBN flakes. The completed hBN/BP/hBN stacks are released onto $\mathrm{Si}/\mathrm{SiO_2}$ wafers with prepatterned local metal gates that are either continuous or split with a ∼150-nm-wide gap. All exfoliation and transfer steps are completed inside a glove box, with moisture and oxygen concentration lower than 0.1 ppm. The stack is patterned into Hall bar geometry by $\mathrm{SF_6}$ plasma reactive-ion etching (RIE), with a metal gate located across the center of the Hall bar. Contacts to BP are made by patterning with electron-beam lithography and RIE that etches only the top hBN layer. A schematic of device is shown in Fig. 1(a). The metal gate controls the charge density of the central region of the device, while the Si back gate controls that of the two outer regions. The devices are characterized at temperature $T = 0.3\,\mathrm{K}$ using standard ac lock-in techniques.

Figure 1(b) displays longitudinal resistance R_{xx} of device $D1$, which has quantum mobility ∼1500 $\mathrm{cm}^2/\mathrm{V\,s}$, as a function of voltages applied to the Si back gate V_{bg} and the metal gate V_{mg}. When either of the gate voltages is close to 0, the device is undoped and insulating; when the gate voltages

*jeanielau1@gmail.com

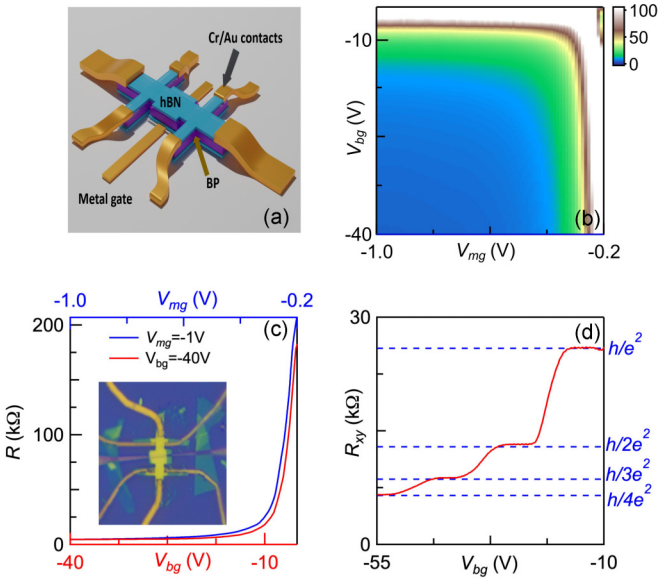

FIG. 1. (a). Schematics of few-layer BP devices. (b). Longitudinal resistance in unit of kΩ R_{xx} vs voltages applied to metal gate V_{mg} and Si back gate V_{bg}. (c). Line traces $R_{xx}(V_{bg})$ at $V_{mg} = -1$ V (red line, bottom axis) and $R_{xx}(V_{mg})$ at $V_{bg} = -40$ V. Inset: optical image of a device. (d). Hall resistance vs V_{bg} at $B = 30$ T, showing well-quantized QH plateaus at filling factors -1, -2, -3, and -4.

decreases, the device becomes highly hole or p doped as its resistance decreases to a few kΩ. Figure 1(c) displays a representative line trace from the color plot—$R_{xx}(V_{bg})$ at $V_{mg} = -1$ V is plotted as the red curve against the bottom axis, whereas $R_{xx}(V_{mg})$ at $V_{bg} = -40$ V is plotted as a blue curve against the top axis. The inset of Fig. 1(c) is an optical image of a typical device. Thus the device acts as a tunable p-$p\prime$-p junction, where resistance of the central and the flanking regions can be separately tuned through several orders of magnitude, from undoped and insulating to highly hole doped and conductive. At high magnetic fields, well-defined QH states are resolved [9,13,25,26]. Figure 1(d) displays $R_{xy}(V_{bg})$ of the side regions at $V_{mg} = -6$ V and $B = 30$ T, where well-quantized resistance plateaus at filling factors $\nu = -1$, -2, -3, and -4 are observed. We note that even though BP is anisotropic, no anisotropy is observed once it enters the QH regime [27].

To examine the equilibration of QH edge states, we measure $D1$'s two-terminal conductance G at $B = 30$ T as V_{bg} and V_{mg} vary. Figure 2(a) displays the resultant data, where the filling factors of the metal-gated region ν_{mg} and of the Si-gated regions ν_{bg} are labeled on the right and top axes, respectively. In the 2D color plot, the data appear as a plaid of colored squares, indicating that the regions are only controlled by a single gate, as expected. The conductance values depend on the filling factors of both regions. We first focus on the regime where $|\nu_{mg}| > |\nu_{bg}|$, and the central region acts as a scatterer for the incident edge states. In the simplest and most common scenario, charge carriers in the central region are equally partitioned among all modes present, regardless of their origination or quantum numbers such as spin, valley and Landau-level indices [28–34]. The resultant conductance is smaller than either filling factor, and is often quantized at a fractional value of the conductance quantum e^2/h, where e is the electron charge and h is the Planck constant. Thus, within the model of full edge state equilibration, the two-terminal conductance of a p-$p\prime$-p junction is given by [29]

$$G\left(\text{in units of } \frac{e^2}{h}\right) = \begin{cases} |\nu_{mg}|, & |\nu_{bg}| \geqslant |\nu_{mg}| \\ \frac{|\nu_{mg}||\nu_{bg}|}{2|\nu_{mg}|-|\nu_{bg}|}, & |\nu_{bg}| \leqslant |\nu_{mg}| \end{cases} \quad (1)$$

(the case of $|\nu_{bg}| \geqslant |\nu_{mg}|$ will be discussed at the end of the paper).

Figure 2(b) illustrates $G(\nu_{bg}, \nu_{mg})$ calculated using Eq. (1), where the expected plateau values are displayed as numbers within each square. The experimental data of $G(\nu_{bg})$ at $\nu_{mg} = -2$ and -4 are shown in Fig. 2(c), and corresponding theoretical curves are shown as dotted lines. Similar plots for $G(\nu_{mg})$ at constant ν_{bg} are displayed in Fig. 2(d). The data are in excellent agreement with those expected from Eq. (1), thus suggesting full equilibration of QH edge states in this few-layer BP device. Some features in the data that are not captured by the equation, such as the small deviation of the plateau values and the resistance dips and finite transition width between the plateaus, may be attributed to impurity scattering and disorder-induced Landau-level broadening [35,36].

We now turn to a different device ($D2$) with higher mobility, $\sim 2500\,\text{cm}^2/\text{V s}$. It differs from device $D1$ in that it has a split (instead of continuous) metal gate. Nevertheless, this device also functions as a p-$p\prime$-p junction, since the narrow gap between the split gates ($\sim$150 nm) is considerably smaller than the width of the depletion (compressible) stripes [37], which is $l \sim \frac{V_g \epsilon}{4\pi^2 ne} \sim 250$ nm, for typical operating parameters. This behavior is also verified in the regime of $|\nu_{mg}| < |\nu_{bg}|$, where both devices display exactly the same behavior (see Fig. 5 and associated discussion).

Figure 3(a) plots the device's two-terminal conductance in unit of e^2/h as a function of V_{mg} and V_{bg}, where the dashed lines denote a partition of regions of different filling factors. The corresponding map calculated from Eq. (1) is shown in the left panel of Fig. 3(b). We first focus on regions with $\nu_{bg} = -1$, i.e., the vertical light blue stripe that is centered at $V_{bg} \sim -9$ V. As shown by the line cut in Fig. 3(c), $G = 1$ for $\nu_{mg} = -1$, which is expected, as the entire device is tuned into the $\nu = -1$ QH state with a single chiral edge channel. However, the $G = 1$ plateau persists to $\nu_{mg} = -2$, contradicting Eq. (1) that predicts $G = 2/3$ [blue dotted line in Fig. 3(c)]; at $\nu_{mg} = -3$, data indicate $G = 0.7$ whereas Eq. (1) predicts 0.6. Such deviation between data and Eq. (1) is also observed for the region ($\nu_{bg} = -2$, $\nu_{mg} = -3$) [Fig. 3(d)], where the data and calculations based on Eq. (1) are shown as red solid and blue dotted lines, respectively.

The disagreement between the data and Eq. (1) prompts us to re-evaluate the assumption of full equilibration. In high mobility devices, QH states with different quantum numbers may not fully equilibrate, due to finite spatial separations and/or the absence of scatterers that can flip the quantum number. For instance, previous works in graphene reported edge states that only equilibrate with the same spin polarization [38] or Landau-level (orbital) index [34]. In our case, the deviation from Eq. (1) is observed within the lowest Landau level. Thus we explore the scenario of spin-selective partial equilibration,

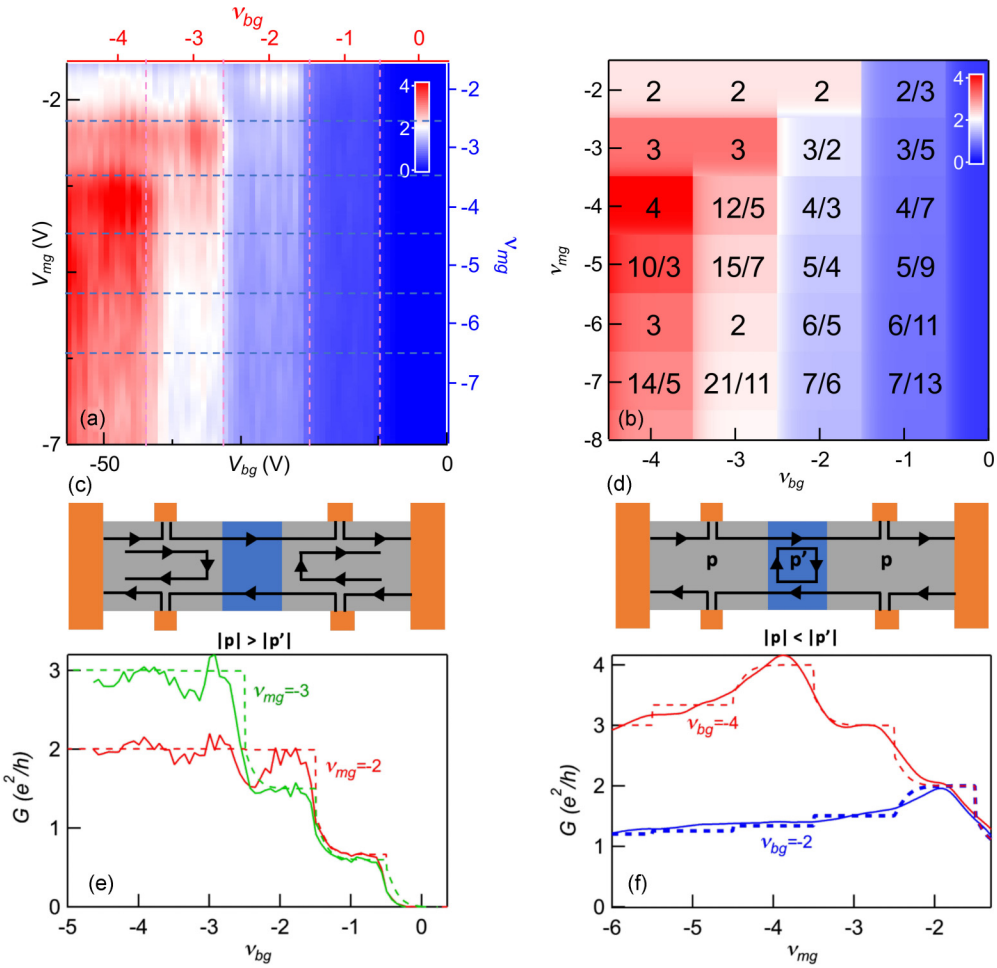

FIG. 2. (a) Conduction G of device $D1$ (in unit of e^2/h) vs back gate voltage V_{bg} and metal gate voltage V_{mg} at $B = 30$ T; the filling factors of metal-gated region ν_{mg} and of the back-gated regions ν_{bg} are labeled on the right and top axes, respectively. (b) Calculated $G(\nu_{bg}, \nu_{mg})$ using Eq. (1), where the number within each square corresponds to expected conductance plateau values. (c), (d) Schematic of edge state transport when $|\nu_{mg}| < |\nu_{bg}|$ and $|\nu_{mg}| > |\nu_{bg}|$, respectively. (e) Experimental data $G(\nu_{bg})$ at $\nu_{mg} = -2$ and -3 (solid lines) and corresponding theoretical curves (dashed lines); (f) $G(\nu_{mg})$ at $\nu_{bg} = -2$ and $\nu_{bg} = -4$ (solid lines) and corresponding theoretical curves (dashed lines).

i.e., equilibration is only achieved among edge states with the same spin, and absent among ones with different spins. In this scenario, $G = G_\uparrow + G_\downarrow$, where $G_\uparrow$ and $G_\downarrow$ are obtained by applying Eq. (1) to spin-up and spin-down edge states, respectively. For instance, for the case $\nu_{bg} = -1$ and $\nu_{mg} = -2$, the spin-up and spin-down edge states do not interact in the central region; hence, the single spin-up state is fully transmitted, while the single spin-down channel is localized within the central region and does not contribute to the conductance. This results in a total conductance of 1 e^2/h, in agreement with data. Similarly, for the case $\nu_{bg} = -2$ and $\nu_{mg} = -3$, the spin-up (spin-down) channel consists of 1 (1) and 2 (1) edge states in the outer and central regions, respectively, giving rise to $G_\uparrow = 2/3$ and $G_\downarrow = 1$, and a total conductance of 5/3 e^2/h [Fig. 3(d) inset].

Using this model, the calculated G values are shown in the right panel of Fig. 3(b), and as red dotted lines in Figs. 3(c) and 3(d). They are in much better agreement with the data than the full equilibration model, thus establishing that equilibration is only achieved among each spin species. At first glance, the different equilibration process in the two devices might be surprising, considering the relatively modest increase in the magnitude of mobility (albeit 70% increase). However, mobility characterizes overall (and mostly bulk) scattering in the device; equilibration of the edge states depends on scatterers *close to the sample edges* and the *interfaces at the p-p′ junctions*. Thus mobility is a relevant, albeit incomplete, metric for the equilibration process here.

Validity of this model is further verified by four-terminal resistance measurements of $D2$, where the metal-gated region is located between the two voltage probes. The longitudinal resistance is given by

$$R_{xx} = \frac{h}{e^2}\left|\frac{1}{|\nu_{mg}|} - \frac{1}{|\nu_{bg}|}\right| \tag{2}$$

for the full equilibration model, and

$$R_{xx} = \frac{r}{T}\frac{1}{|\nu_{bg}|}\frac{h}{e^2} \tag{3}$$

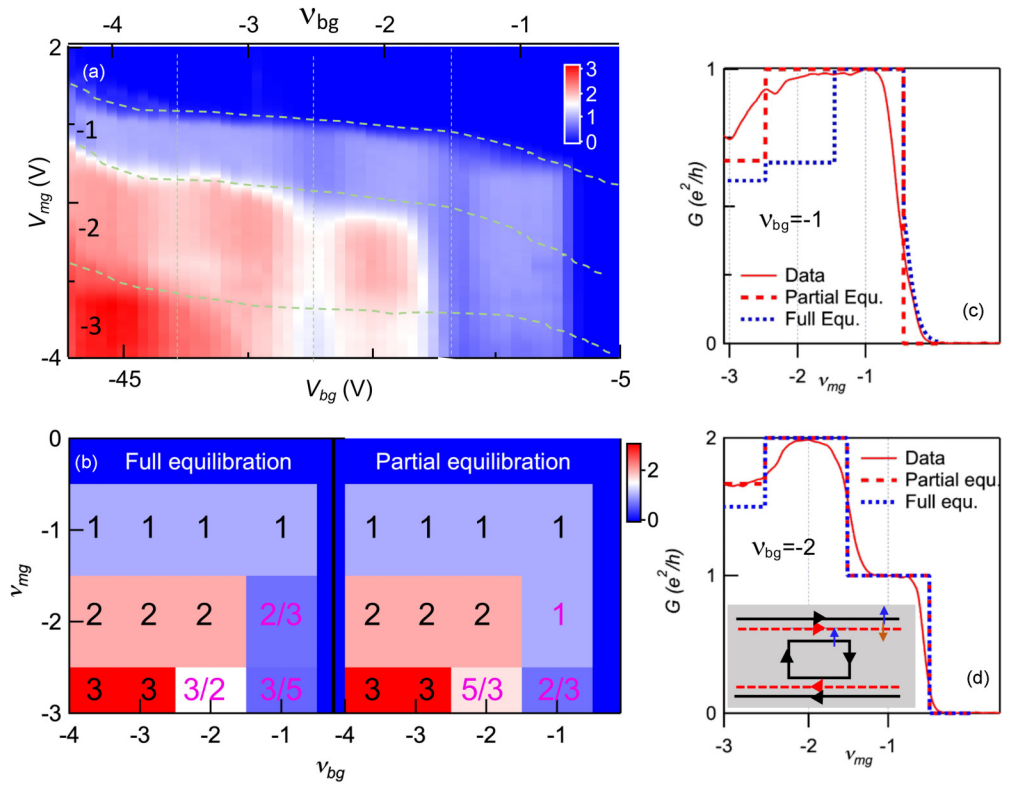

FIG. 3. (a) Two-terminal conductance G of device $D2$ (in unit of e^2/h) vs back gate voltage V_{bg} and metal gate voltage V_{mg} at $B = 30$ T. The filling factors of metal-gated region ν_{mg} and of the back-gated regions ν_{bg} are labeled on the left and top axes, respectively. The dashed lines are drawn to approximately delineate regions with different filling factors. (b) Calculated $G(\nu_{bg}, \nu_{mg})$ using full equilibration (left panel) and partial equilibration model (right panel), respectively. (c) Experimental data $G(\nu_{mg})$ (red solid line), theoretical curve using full equilibration model (blue dotted line), and theoretical curve using partial equilibration model (red dashed line) at $\nu_{bg} = -1$. (d) Similar to (c), except at $\nu_{bg} = -2$. Inset: Schematic of edge states with spin polarizations.

for partial equilibration, where $T = \frac{G_\uparrow + G_\downarrow}{|\nu_{bg}|}$ is the overall transmission coefficient for the $|\nu_{bg}|$ incoming channels, and $r = 1 - T$ is the reflection coefficient. Figure 4(a) displays the $R_{xx}(\nu_{bg}, \nu_{mg})$ map calculated according to Eq. (3), and Fig. 4(b) displays the experimental data. Figures 4(c) and 4(d) plot line traces $R_{xx}(\nu_{mg})$ at $\nu_{bg} = -1$ and -2, respectively, as well as expected values calculated from Eq. (2) (blue dashed lines) and Eq. (3) (red dotted lines). The data are most consistent with the partial equilibration model, again confirming spin-based equilibration.

Last, we investigate the regime with relatively large $|\nu_{bg}|$ so that $|\nu_{mg}| \langle |\nu_{bg}|$, and the central region hosts a smaller number of edge states than the outer regions. Here only $|\nu_{mg}|$ edge states are fully transmitted from source to drain, whereas the rest are reflected. Therefore the conductance is given by the upper equation of Eq. (1), and expected values are shown in Figs. 2(b) and 3(b). Figures 5(a) and 5(b) plot $G(\nu_{mg})$ at $\nu_{bg} = -4$ and -5 for devices $D1$ and $D2$, respectively. In both graphs, as $|\nu_{mg}|$ is lowered, G decreases stepwise from $|\nu_{mg}| = |\nu_{bg}|$ to 0, indicating that the edge channels are filtered out one by one, until conductance is completely turned off. Thus, in this regime, the p-p'-p junction serves as a "filter" for the edge channels, similar to the pinch-off of edge states by quantum point contacts in GaAs-based heterostructures. Such gate-tunable filters of edge states can be used to construct quantum computation platforms based on interferometry of edge states.

In summary, using dual-gated few-layer BP devices, we demonstrate that they function as p-p'-p junctions with tunable charge densities in each region. In the QH regime, when the central region hosts a larger number of edge states than the outer regions, the circulating edge states therein couple modes that have different electrochemical potentials. We observe both full equilibration, where all modes equilibrate and are partitioned equally at the p-p' interfaces, and partial equilibration, where modes only equilibrate among the same spin polarization. When the central region hosts fewer edge states than the outer region, the junction behaves as a filter so as to enable stepwise, gate-tunable transmission of integer quantum Hall edge channels. These results underscore the potential of BP and 2D semiconductors as a versatile platform for understanding and manipulating QH physics and other topological edge states.

This work was supported by NSF/ECCS Grant No. 1509958 and NSF/DMR Grant No. 1807928. A portion of

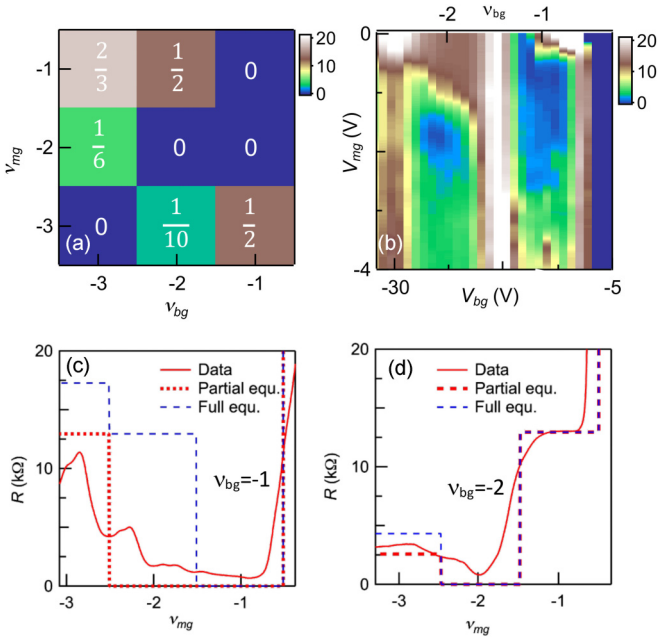

FIG. 4. (a) Calculated $R_{xx}(\nu_{bg}, \nu_{mg})$ map using Eq. (3). (b) Longitudinal resistance $R_{xx}(V_{mg}, V_{bg})$ of device $D2$ at $B = 30$ T. (c) Experimental data $R_{xx}(\nu_{mg})$ (red solid line), theoretical curve using full equilibration model (blue dashed line), and theoretical curve using partial equilibration model (red dotted line) at $\nu_{bg} = -1$. (d) Similar to (c), except at $\nu_{bg} = -2$.

this work was performed at the National High Magnetic Field Laboratory, which is supported by National Science Foundation Cooperative Agreement No. DMR-1157490 and the State of Florida. K.W. and T.T. acknowledge support from the Elemental Strategy Initiative conducted by MEXT, Japan, Grant No. JPMXP0112101001, JSPS KAKENHI Grant No. JP20H00354, and the CREST (Grant No. JPMJCR15F3), JST.

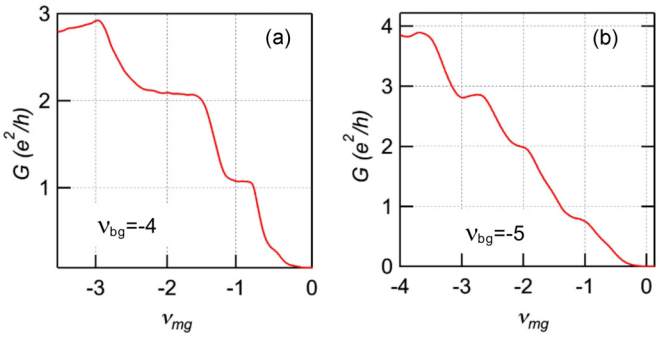

FIG. 5. (a) $G(\nu_{mg})$ at $\nu_{bg} = -4$ for device $D1$. (b) $G(\nu_{mg})$ at $\nu_{bg} = -3$ for device $D2$.

[1] R. E. Prange and S. M. Girvin, *The Quantum Hall Effect*, edited by R. E. Prange and S. M. Girvin, Foreword by Klaus von Klitzing (Springer-Verlag, New York, 1988).

[2] T. J. Witt, Electrical resistance standards and the quantum Hall effect, Rev. Sci. Instrum. **69**, 2823 (1998).

[3] C. de C. Chamon, D. E. Freed, S. A. Kivelson, S. L. Sondhi, and X. G. Wen, Two point-contact interferometer for quantum Hall systems, Phys. Rev. B **55**, 2331 (1997).

[4] S. D. Sarma and A. Pinczuk, *Perspectives in Quantum Hall Effects: Novel Quantum Liquids in Low-Dimensional Semiconductor Structures* (Wiley-VCH, Hoboken, NJ, 1996).

[5] B. Lian, X.-Q. Sun, A. Vaezi, X.-L. Qi, and S.-C. Zhang, Topological quantum computation based on chiral Majorana fermions, Proc. Natl. Acad. Sci. U.S.A. **115**, 10938 (2018).

[6] R. S. K. Mong, D. J. Clarke, J. Alicea, N. H. Lindner, P. Fendley, C. Nayak, Y. Oreg, A. Stern, E. Berg, K. Shtengel, and M. P. A. Fisher, Universal Topological Quantum Computation from a Superconductor-Abelian Quantum Hall Heterostructure, Phys. Rev. X **4**, 011036 (2014).

[7] X.-G. Wen, theory of the edge states in fractional quantum hall effects, Int. J. Mod. Phys. B **6**, 1711 (1992).

[8] Y. Zhang, Y.-W. Tan, H. L. Stormer, and P. Kim, Experimental observation of the quantum Hall effect and Berry's phase in graphene, Nature (London) **438**, 201 (2005).

[9] S. Tran, J. Yang, N. Gillgren, T. Espiritu, Y. Shi, K. Watanabe, T. Taniguchi, S. Moon, H. Baek, D. Smirnov, M. Bockrath, R. Chen, and C. N. Lau, Surface transport and quantum Hall effect in ambipolar black phosphorus double quantum wells, Sci. Adv. **3**, e1603179 (2017).

[10] D. Wang, S. Che, G. Cao, R. Lyu, K. Watanabe, T. Taniguchi, C. N. Lau, and M. Bockrath, Quantum Hall Effect Measurement of Spin–Orbit Coupling Strengths in Ultraclean Bilayer Graphene/WSe2 Heterostructures, Nano Lett. **19**, 7028 (2019).

[11] Y. Lee, J. Velasco, D. Tran, F. Zhang, W. Bao, L. Jing, K. Myhro, D. Smirnov, and C. N. Lau, Broken symmetry quantum Hall states in dual-gated ABA trilayer graphene, Nano Lett. **13**, 1627 (2013).

[12] H. Liu, A. T. Neal, Z. Zhu, Z. Luo, X. Xu, D. Tománek, and P. D. Ye, Phosphorene: An Unexplored 2D Semiconductor with a High Hole Mobility, ACS Nano **8**, 4033 (2014).

[13] J. Yang, S. Tran, J. Wu, S. Che, T. Taniguchi, K. Watanabe, H. Baek, D. Smirnov, R. Chen, and C. N. Lau, Integer and fractional quantum hall effect in ultra-high quality few-layer black phosphorus transistors, Nano Lett. **18**, 229 (2018).

[14] L. K. Li, Y. J. Yu, G. J. Ye, Q. Q. Ge, X. D. Ou, H. Wu, D. L. Feng, X. H. Chen, and Y. B. Zhang, Black phosphorus field-effect transistors, Nat. Nanotechnol. **9**, 372 (2014).

[15] T. Low, A. S. Rodin, A. Carvalho, Y. Jiang, H. Wang, F. Xia, and A. H. C. Neto, Tunable optical properties of multilayer black phosphorus thin films, Phys. Rev. B **90**, 075434 (2014).

[16] J. Qiao, X. Kong, Z.-X. Hu, F. Yang, and W. Ji, High-mobility transport anisotropy and linear dichroism in few-layer black phosphorus, Nat. Commun. **5**, 4475 (2014).

[17] A. S. Rodin, A. Carvalho, and A. H. Castro Neto, Strain-Induced Gap Modification in Black Phosphorus, Phys. Rev. Lett. **112**, 176801 (2014).

[18] A. Castellanos-Gomez, Black phosphorus: Narrow gap, wide applications, J. Phys. Chem. Lett. **6**, 4280 (2015).

[19] J. Kim, S. S. Baik, S. H. Ryu, Y. Sohn, S. Park, B.-G. Park, J. Denlinger, Y. Yi, H. J. Choi, and K. S. Kim, Observation of tunable band gap and anisotropic Dirac semimetal state in black phosphorus, Science **349**, 723 (2015).

[20] V. Tran, R. Soklaski, Y. Liang, and L. Yang, Layer-controlled band gap and anisotropic excitons in few-layer black phosphorus, Phys. Rev. B **89**, 235319 (2014).

[21] H. Liu, Y. Du, Y. Deng, and P. D. Ye, Semiconducting black phosphorus: synthesis, transport properties and electronic applications, Chem. Soc. Rev. **44**, 2732 (2015).

[22] X. Ren, Z. Li, Z. Huang, D. Sang, H. Qiao, X. Qi, J. Li, J. Zhong, and H. Zhang, Environmentally robust black phosphorus nanosheets in solution: Application for self-powered photodetector, Adv. Funct. Mater. **27**, 1606834 (2017).

[23] X. Ling, H. Wang, S. Huang, F. Xia, and M. S. Dresselhaus, The renaissance of black phosphorus, Proc. Natl. Acad. Sci. U.S.A. **112**, 4523 (2015).

[24] F. Xia, H. Wang, and Y. Jia, Rediscovering black phosphorus as an anisotropic layered material for optoelectronics and electronics, Nat. Commun. **5**, 4458 (2014).

[25] L. Li, F. Yang, G. J. Ye, Z. Zhang, Z. Zhu, W. Lou, X. Zhou, L. Li, K. Watanabe, T. Taniguchi, K. Chang, Y. Wang, X. H. Chen, and Y. Zhang, Quantum Hall effect in black phosphorus two-dimensional electron system, Nat. Nanotechnol. **11**, 593 (2016).

[26] G. Long, D. Maryenko, J. Shen, S. Xu, J. Hou, Z. Wu, W. K. Wong, T. Han, J. Lin, Y. Cai, R. Lortz, and N. Wang, Achieving ultrahigh carrier mobility in two-dimensional hole gas of black phosphorus, Nano Lett. **16**, 7768 (2016).

[27] See Supplemental Material at http://link.aps.org/supplemental/10.1103/PhysRevMaterials.4.114008 for additional data on the absence of anisotropic transport in the quantum Hall regime and comparison of two- and four-terminal measurements.

[28] D. L. Kovrizhin and J. T. Chalker, Equilibration of integer quantum Hall edge states, Phys. Rev. B **84**, 085105 (2011).

[29] B. Ozyilmaz, P. Jarillo-Herrero, D. Efetov, D. A. Abanin, L. S. Levitov, and P. Kim, Electronic Transport and Quantum Hall Effect in Bipolar Graphene p-n-p Junctions, Phys. Rev. Lett. **99**, 166804 (2007).

[30] C. Lin, R. Eguchi, M. Hashisaka, T. Akiho, K. Muraki, and T. Fujisawa, Charge equilibration in integer and fractional quantum Hall edge channels in a generalized Hall-bar device, Phys. Rev. B **99**, 195304 (2019).

[31] B. W. Alphenaar, P. L. McEuen, R. G. Wheeler, and R. N. Sacks, Selective equilibration among the current-carrying states in the quantum Hall regime, Phys. Rev. Lett. **64**, 677 (1990).

[32] J. R. Williams, L. DiCarlo, and C. M. Marcus, Quantum hall effect in a gate-controlled p-n junction of graphene, Science **317**, 638 (2007).

[33] D. A. Abanin and L. S. Levitov, Quantized transport in graphene p-n junctions in a magnetic field, Science **317**, 641 (2007).

[34] N. N. Klimov, S. T. Le, J. Yan, P. Agnihotri, E. Comfort, J. U. Lee, D. B. Newell, and C. A. Richter, Edge-state transport in graphene p–n junctions in the quantum Hall regime, Phys. Rev. B **92**, 241301(R) (2015).

[35] Z. Li and J. P. Carbotte, Particle-hole asymmetry on Hall conductivity of a topological insulator, Phys. Rev. B **89**, 085413 (2014).

[36] C. Gneiting, Z. Li, and F. Nori, Lifetime of flatband states, Phys. Rev. B **98**, 134203 (2018).

[37] D. B. Chklovskii, B. I. Shklovskii, and L. I. Glazman, Electrostatics of edge channels, Phys. Rev. B **46**, 4026 (1992).

[38] F. Amet, J. R. Williams, K. Watanabe, T. Taniguchi, and D. Goldhaber-Gordon, Selective Equilibration of Spin-Polarized Quantum Hall Edge States in Graphene, Phys. Rev. Lett. **112**, 196601 (2014).

Correction: A notice of inclusion in the collection titled Two-Dimensional Materials and Devices was missing and has been inserted.